PERGAMON

International Journal of Multiphase Flow 26 (2000) 1951–1979

International Journal of Multiphase Flow

www.elsevier.com/locate/ijmulflow

Gas cluster growth by solute diffusion in porous media. Experiments and automaton simulation on pore network

A. Dominguez, S. Bories*, M. Prat*

Institut de Mecanique des Fluides de Toulouse, UMR CNRS-INP/UPS No. 5502, Avenue du Professeur Camille Soula, F-31400 Toulouse, France

Received 13 February 1999; received in revised form 28 December 1999

Abstract

The study presented in this paper deals with the liquid–gas phase change by pressure decline of supersaturated CO_2 solutions in 2D porous media. The growth of the gas phase is studied experimentally and numerically as a function of supersaturation, wettability and gravity. Experiments are performed on a transparent etched network (micromodel) and simulations with a specific numerical automaton.

In the experiments, the nucleation process, i.e. the occurrence of the gas bubbles, as well as the growth of these bubbles are visualised and analysed by means of a micro video camera and an image processing apparatus. The observations confirm the heterogeneous nature of nucleation and the disordered growth pattern of the gas phase. The analysis of the growth rate of a single gas cluster shows that this phenomenon is different from the compact growth of an isolated single bubble in the bulk. As previously predicted, the bubble growth by mass transfer and volume expansion in porous media is characterised by a pattern of the invasion percolation type under normal laboratory conditions.

Numerical simulations of the growth pattern and the growth rate of a single gas cluster are performed with a numerical automaton. Based on a pore network modelling technique and a set of hypotheses derived from the observations, this automaton is first validated by comparing the numerical results with the experiments. Then, the automaton is used to conduct a sensitivity study. In particular, the influences of the Jakob number, pressure decline rate, Bond number, wettability and characteristics of the microstructure are investigated.

Keywords: Porous medium; Nucleation; Bubble growth; Pore network; Experiments; Simulation

* Corresponding authors.
E-mail addresses: bories@imft.fr (S. Bories), prat@imft.fr (M. Prat).

0301-9322/00/$ - see front matter
PII: S0301-9322(00)00006-9

1. Introduction

The liquid–vapor phase change by pressure decline or superheat in porous media is an important problem encountered in different applications such as porous surface boiling, geothermal systems, drying of materials, thermal methods for oil recovery. As in the case of homogeneous liquids, this phenomenon is described by the two main consecutive processes: (i) bubble nucleation, which appears when the pressure decreases under the saturation value (Zettlemoyer, 1969), (ii) bubble growth due to the mass diffusion driven by pressure lowering or by heat conduction (Scriven, 1959). Contrary to this case, however, relatively few studies have been conducted to quantify these processes in fluid saturated porous media and particularly to analyse the influence of geometry and topology of the microstructure on the rate of gas generation. Moreover, among the studies devoted to this problem, most of them have been inconclusive until now (Hunt and Berry, 1956; Moulu, 1989; Kashchief and Firoozabadi, 1993)

As summarised in Li and Yortsos (1994) and following the visualisations presented in El-Yousfy (1992) and Li and Yortsos (1995), the origin of difficulties encountered in analysing the previous investigations has been identified. They mainly result from: (i) the approach used to conduct the analysis, i.e. the macroscopic approach based on the identification of the liquid-saturated porous medium with a continuum, (ii) the use of models valid only in the bulk liquid phase to describe the nucleation and phase growth in porous media. Given the presence of the solid microstructure and the geometric complexity of the pore space that bounds the flow domain and constrain the growth of the gas phase, this approach is questionable.

In order to address porous media effects, certain aspects of nucleation and bubble growth have been recently studied experimentally, numerically and theoretically in simplified 2D porous structures, (El-Yousfy et al., 1991; Li and Yortsos, 1994, 1995). These studies, which concern the phenomenology of nucleation and growth of the gas phase, are based on visualisations of the liberation of CO_2 gas from various supersaturated carbonate liquids (via solute diffusion) in transparent micromodels, on pore network numerical simulations and on scaling arguments. The visualisations confirmed the existence of specific nucleation sites, the growth of bubbles in the form of ramified clusters and the influence of capillary effects on the growth process, cf. El-Yousfy et al. (1991), El-Yousfy (1992) and Li (1993). On the basis of these observations, it was concluded that a single gas cluster first grows in a manner similar to an invasion percolation process (El-Yousfy, 1992; Li, 1993). However, as discussed in Satik et al. (1995), when the size of the cluster becomes sufficiently large, deviations from a percolation pattern are expected owing to the influence of viscous effects. The viscous effects are negligible in the present study which therefore, focuses on invasion percolation growth patterns.

The present paper continues and extends the work of El-Yousfy et al. (1991), El-Yousfy (1992) and Li (1993) concerning the nucleation and the gas cluster growth by solute diffusion in porous media. While in these previous studies, attention was essentially focussed on the influence of supersaturation and of pressure decline rate on growth, in the present work, we provide, insights into the effects of wettability, gravity and correlated microstructures.

The experiments were performed in a transparent pore network model saturated with

different CO_2–liquid solutions initially in equilibrium at $Po = 3$ bar. For the purpose of understanding the specific influence of pore geometry on the bubble growth pattern, experiments were also carried out in a transparent Hele-Shaw cell. Bubble growth in a Hele-Shaw cell is expected to be analogous to the growth predicted by classical (macroscopic) two dimensional porous media models. Results derived from pressure measurements and from image analysis of direct optical visualisations can be related to mechanisms of nucleation and bubble growth. A part of these results was used to build a network automaton intended to simulate the process numerically under various conditions. This automaton is briefly described and verified through direct numerical simulation of the experiments. Prior to this description and to the discussion of simulations we focus on the experimental study and the physical analysis of the underlying phenomena.

2. Experiments

2.1. Experimental set-up

In order to obtain an insight into the micromechanics of the process and to test the theoretical predictions, a series of experiments were carried out. These experiments were performed on a 2D transparent resin Hele-Shaw cell and on a transparent pore network model (micromodel) initially saturated with solutions of CO_2 in various liquids in equilibrium at a pressure $Po = 3$ bar. The micromodel with a plan form of 15×14 cm^2 consisted in a regular square lattice pattern of 42,000 rectangular ducts of 700 μm uniform thickness, and variable width. The lattice spacing is 1 mm and the widths of ducts, varying in the range from 200 to 800 μm, obey a prescribed log-normal distribution law which corresponds to a typical pore size distribution function of a real porous medium. The Hele-Shaw cell has the same size as the micromodel (15×14 cm^2) and a thickness of 700 μm. A gas tank and a flow controller were used to impose the pressure decline rate. A video microcamera connected to an image processing apparatus was used to obtain quantitative data from the observation of the bubbles and clusters inside the micromodel. The schematic of the experimental set-up is shown in Fig. 1.

The experimental procedure was as follows. CO_2 was first injected into the micromodel to displace the air. Pure liquid (water, n-octane, n-decane, water–glycol solutions, as listed in Table 1) was then injected to dissolve CO_2 and to pressurize the model typically at $Po = 3$ bar. Finally, the pure liquid was displaced by the CO_2 solution. Once the liquid–CO_2 solution was

Table 1
Fluid physical properties

	K (mol m^{-1} N^{-1})	σ (N m^{-1})	D (m^2 s^{-1})	μ Poiseuille	ρ (kg m^{-3})
(A) Octane	5×10^{-4}	21.80×10^{-3}	4.97×10^{-9}	0.510×10^{-1}	0.70×10^{3}
(B) Decane	4×10^{-4}	23.43×10^{-3}	3.90×10^{-9}	0.850×10^{-1}	0.75×10^{3}
(C) Xglycol = 0.5	3.21×10^{-4}	53.02×10^{-3}	0.60×10^{-9}	7.00×10^{-1}	1.10×10^{3}
(D) Xglycol = 0.2	2.63×10^{-4}	58.06×10^{-3}	1.00×10^{-9}	3.00×10^{-1}	1.01×10^{3}

in place inside the micromodel, the micromodel and the connected tanks were maintained at $P = 3.5$ bar for many hours in order that the solution homogenises. The experiments were then performed by reducing, either suddenly or with various constant rates ($m = -\mathrm{d}P/\mathrm{d}t$), the initial liquid pressure from $Po = 3$ bar to P_∞, with $Po - P_\infty = \Delta P > 0$, by means of a microelectronic valve (denoted by m.e. in Fig. 1). During the experiments, the pressure and volume of the solution flowing out of the micromodel to the separator of phases through two outlets situated in the middle of the two lateral sides, were measured as a function of time, and the processes of nucleation and growth were videotaped by means of a camera connected to a VCR and a PC. The images were digitised and an image processing software (Visilog 4) was used to analyse the phase distribution. Experiments were stopped shortly after the gas started to come out from the micromodel.

2.2. Results

2.2.1. Appearance of bubbles

El-Yousfy (1992) and Dominguez (1997) have recently carried out studies with fixed liquid

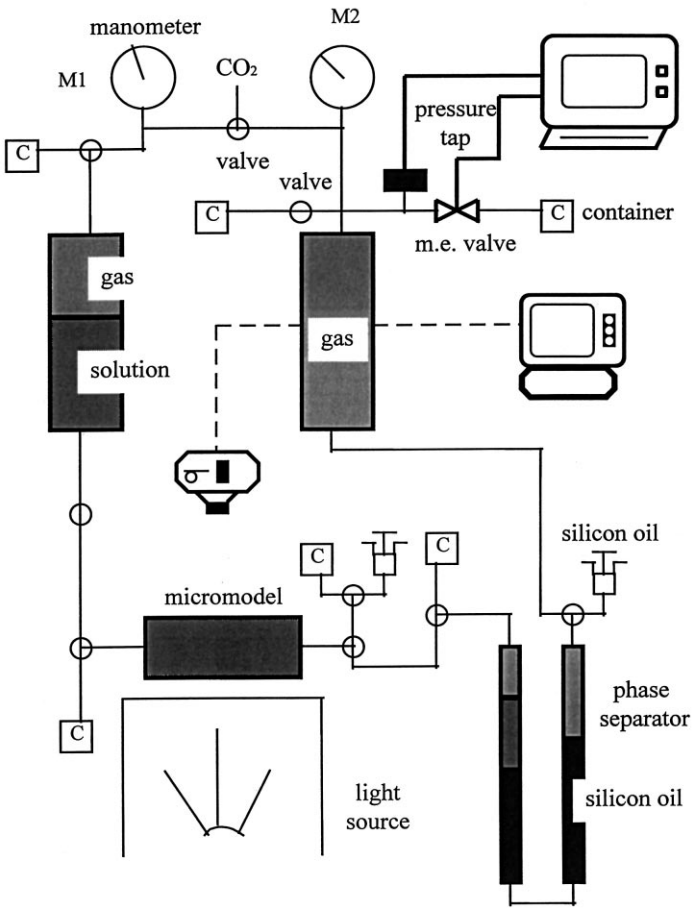

Fig. 1. Schematic diagram of the experimental set-up.

supersaturation ($\Delta C = K\Delta P$ with C = CO_2 concentration, K = solubility constant and ΔP = pressure decline) and showed starting from visualisations of nucleation events at the pore level and quantitative measurements, that the nucleation process in the porous medium under study is presumably due to the pre-existence of stabilised microbubbles in cavities, irregularities and impurities at the surface of pores. This hypothesis was first derived from numerical evaluations based on theoretical results concerning the formation of active nucleation sites as a function of supersaturation, wettability, number density and shapes of the cavities on the solid surfaces (Tong et al., 1990; Wang and Dhir, 1993). The above hypothesis was also reinforced by a set of experimental observations which are in complete contradiction with the classical homogeneous or heterogeneous nucleation theories. These observations by El-Yousfy (1992) include,

1. the formation of nucleation sites on the pores walls,
2. the spatial reproducibility of nucleation sites,
3. the existence of a threshold for bubble appearance,
4. the inverse time of appearance of the first bubble $1/t$ being proportional to the dimensionless supersaturation $\Delta P/Po$ and not to $(\Delta P/Po)^2$, contrary to the classical nucleation laws, and finally,
5. the total number N of bubbles produced in agreement with the Yang's law, cf. Yang and Kim (1988), i.e., $N \propto \exp(-A/\Delta P)$ (with A depending of the properties of the solid surface) derived for the bubbles nucleation from cavities on solid surfaces.

In the present work, we present experimental evidence on the influence of wettability on the rate of bubble appearance that confirms the hypothesis of pre-existence of bubbles in cavities. These experiments, carried out with the same micromodel and for the same pressure lowering

Fig. 2. Distributions of initial gas clusters in a micromodel for various wettability: The number of growth sites decreases with the wettability. The results were obtained for $\Delta P/\Delta P_{sat} = 0.63$ and $\theta = 0.00$ rad (a), $\theta = 0.66$ rad (b) and $\theta = 0.82$ rad (c).

conditions as in El-Yousfy (1992) but for different liquids (the characteristics of which are given in Table 1), clearly demonstrate the decisive influence of the wetting angle θ on the creation of bubbles. The visualisations depicted in Fig. 2 and the results summarised in Table 2 show that more than 500 bubbles are formed for the less wetting solutions (water–CO_2 solutions) while we only observe none or one bubble for the perfectly wetting hydrocarbons solutions. Given the physicochemical properties of the liquids used, these results are in agreement with those that can be deduced from the work of Wang and Dhir (1993) showing the de-activation of nucleation sites as the wettability increases. Consequently, for the supersaturation conditions used, this result confirms the decisive role of the capillary trapping mechanism on the appearance of bubbles, i.e. the pre-existence of microbubbles trapped in cavities, or stabilised by the presence of impurities at the liquid interface of the bubbles.

Contrary to the classical nucleation theories that predict the emergence of bubbles as a spatially random process characterised by a continuous rate of nucleation as a function of supersaturation, bubbles arise here from various sites at the pore walls where the gas is trapped by capillarity. The gas is released when the supersaturation is such that the increase of the gas pressure induced by the mass transfer leads to a local capillary pressure that exceeds the threshold value of the site. Although well known in the field of boiling on rough surfaces, this result was largely controversial up to now in the petroleum engineering literature, Betata (1998). However, the thermodynamical history and the liquid setting within the pore space can be a priori significantly different in a petroleum reservoir from those concerning the laboratory experiments presented here.

2.2.2. Bubble growth

Subsequent to nucleation, bubbles begin to grow within the pore space. This growth occurs until the bubble radius reaches the pore size. If the supersaturation is too large, invasion of surrounding pores by vapor will ensue until an appropriate stabilizing pore geometry is encountered. One can refer to Yortsos and Parlar (1989) for the study of possible equilibrium states.

According to Szekely and Martins (1971), the growth of a vapor bubble in porous media is controlled by forces similar to those in bulk phase change, namely inertia, viscous, surface and pressure forces. In terms of dimensionless groups, this phenomenon can be characterised by the Jakob number, $Ja = \Delta P/Po$, the pressure parameter, $G = a^2\Delta P/\rho_L D^2$ (where ρ_L is the liquid density, D the molecular diffusivity, a is the lattice spacing or the Hele-Shaw cell aperture), the

Table 2
Number of nucleation sites as a function of $\Delta P/P_{sat}$ and θ. Each number in brackets corresponds to an experiment

$\Delta P/P_0$	*n*-Octane $\theta = 0.00$ (rad)	*n*-Decane $\theta = 0.01$ (rad)	Glycol–water mixture, glycol mole fraction = 0.5, $\theta = 0.66$ (rad)	Glycol–water mixture, glycol mole fraction = 0.2, $\theta = 0.82$ (rad)
0.46	(0, 0)	(1)	(23, 21)	(509)
0.56	(0, 0)	(3, 3, 3)	(33, 36)	(> 509)
0.66	(1, 1, 1, 1, 0) (0)	(9, 7, 6)	(50, 46)	(> 509)

surface tension parameter, $\Phi = 2\sigma/a\Delta P$ (σ is the interfacial tension), the Schmidt number $Sc = \eta/D$ (η is the dynamic viscosity), the driving parameter, $\Delta P/P_\infty$, and finally $B = Ja^2/\sqrt{G}$ which occurs in the momentum and mass transfer equations. This last number is a useful indicator of the mechanisms involved in the cluster growth. When $B \ll 1$, the process is diffusion-controlled, whereas for $B \gg 1$ the process is inertia-controlled. As it is well known, inertia control prevails only under severe conditions.

For the growth of a vapor cluster in porous media a modified capillary number, $Ca = \rho_L \nu D/a\sigma\cos(\theta)$, which measures the relative importance of the viscous and capillary forces, and the Bond number, $Bo = \rho_L a^2 g \sin(\phi)/\sigma\cos(\theta)$, which measures the relative importance of gravity effect and capillarity, as well as the pore size function distribution of the microstructure must be taken into consideration. Concerning the pressure decline rate which controls the evolution of supersaturation as a function of time, the corresponding dimensionless number is given by $M = ma^2/PoD$.

For the experiments reported in the present paper, i.e. with the different CO_2 solutions and different physical models (Hele-Shaw cell and micromodels), the values of the dimensionless numbers are in the following ranges: $10 > Ja > 0.6$; $G > 10^{14}$; $\Phi \approx 10^{-2}$; $Ca \approx 10^{-6}$; $Bo \approx 5.10^{-3}$, and $10^2 < Sc < 10^4$. The growth process is therefore diffusion controlled. This result, which concerns the initial stages as well as the advanced stages of the growth, was confirmed experimentally in Hele-Shaw cell as shown in Figs. 3 and 4. As can be seen from Fig. 3, the average dimensionless radius $R^* = R/a$ of the compact gas pattern (cylindrical gas bubble) grows according to the classical 2D diffusion law, i.e. $R^* \propto Ja\tau^{1/2}$ ($\tau = ta^2/D$) for a rapid depressurisation; this law corresponds to the dashed line in Fig. 3. When the transport by convection induced in the liquid by the bubble growth is taken into account, one obtains the solid line shown in Fig. 3, cf. Dominguez (1997). For a linear decay, one expects $R^* \propto M^{1/2}\tau^{3/2}$ when τ tends to the infinity, cf. Wang and Bankoff (1991). As can be seen from Fig. 4, however, the agreement between the theory and the experimental results is not as good as for the rapid depressurisation shown in Fig. 3. This may be due to the limited size of the

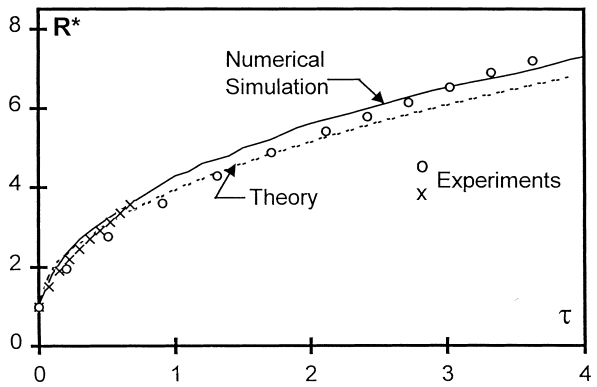

Fig. 3. Influence of Sc/G on the rate of bubble growth in a Hele-Shaw cell with $Ja = 1.65$, (×) $Sc/G = 1.42 \times 10^{-11}$; (○) $Sc/G = 3.40 \times 10^{-11}$. Experimental data (× and ○) are compared with the results corresponding to a pure diffusion transport in the liquid (theory, dashed line) and to the numerical solution including the influence of the transport by convection in the liquid (solid line).

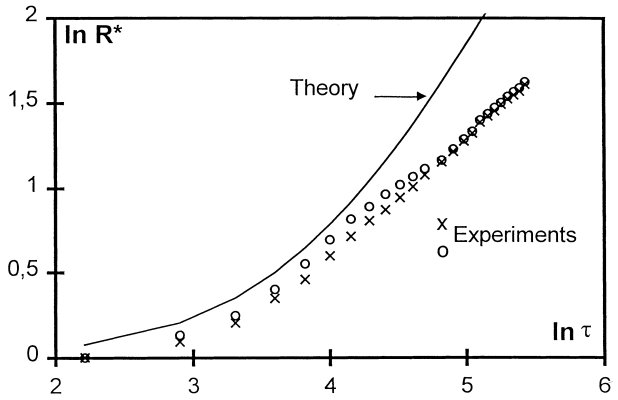

Fig. 4. Bubble growth in a Hele-Shaw cell under a linear increase of gas super-saturation. Experimental data (x, o) for $M = 25 \times 10^{-4}$ versus theoretical values (solid line).

system. Moreover, a sensitivity study based on numerical simulations showed that the growth process was not significantly affected by the liquid convection, the viscous stress on the internal surface of the Hele-Shaw cell and the surface tension in the range of parameters used, cf. Dominguez (1997).

Contrary to the growth in the bulk or in an effective porous medium such as a Hele-Shaw cell where the gas patterns are compact (for instance disk-shaped in the absence of gravity and dissymmetry conditions, as shown in Fig. 5(a), visualisations show that in micromodel (which

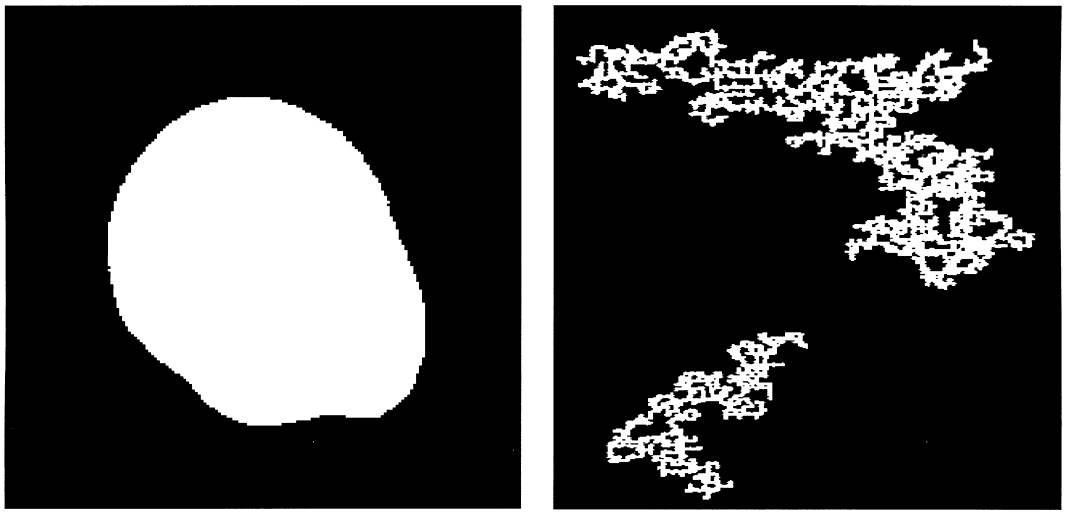

(a) (b)

Fig. 5. Typical shape of a bubble observed in a Hele-Shaw cell (a) and in a micromodel (b) (gas phase in white, liquid phase in black). With the Hele-Shaw cell, one expects in fact, a circular bubble. Small aperture variations may explain the non perfectly circular shape depicted in Fig. 5(a).

mimics real porous media) the shape of the formed gas clusters is clearly disordered and non symmetric (Fig. 5(b)). This complicated but nevertheless reproducible pattern is the result of the influence of the microstructure on the invasion process of the pore space. The menisci along the cluster perimeter are stationary or moving according to whether the capillary pressure is lower or greater than the capillary pressure threshold of the adjacent pore throat, i.e. $Pg - P_\infty = 2\sigma \cos\theta/r$, where r is the equivalent radius of the throat connecting the gas cluster to an adjacent liquid-occupied pore. Visualisation of this growth pattern, which is driven by the supersaturation Ja or the pressure decline rate M and constrained by the specific pore geometry of the porous medium is shown in Fig. 5(b).

For a diffusion-controlled regime, the growth rate of a single gas cluster can be readily estimated from a scale analysis of the diffusion equation. When the supersaturation can be assumed constant in the far field, it is easy to show that the area (equivalent to the volume in micromodels) of a single gas cluster is given by $\Sigma \propto Ja^2 \tau FF$, where $FF = \Gamma^2/4\pi\Sigma$ is called the shape factor, and Γ and Σ are the perimeter of the cluster (proportional to the area of the gas–liquid interface) and the area of the cluster (proportional to the volume), respectively. While $FF = 1$ in the bulk or in an effective 2D porous medium, i.e. for a circular gas bubble growing in a Hele-Shaw cell the result is different in 2D real porous media. As can be seen from Fig. 6, after a transition stage corresponding to the typical growth of the bubble in a single pore (radius of the bubble $\propto \sqrt{t}$, cf. El-Yousfy, 1992), this coefficient tends to increase as a function of time. Consequently, for the same values of Ja, the same boundaries conditions and $Bo = 0$, the volume of a single gas cluster tends to grow faster in a real porous medium than in a Hele-Shaw cell or an effective porous media. Similar conclusions were derived by Satik et al. (1995). They concluded that the pattern exhibits a fractal structure and proposed an explicit scaling law to describe the gas cluster growth in the percolation domain. This law was derived under the assumption of quasistatic concentration fields and is expressed by

$$(R/a)^{\lambda}\big(1 + \lambda \ln(\mathrm{Re}/R)\big)2\pi k\lambda\tau \tag{1}$$

where R is the cluster radius of giration (see, for instance, Stauffer and Aharony, 1992), Re the

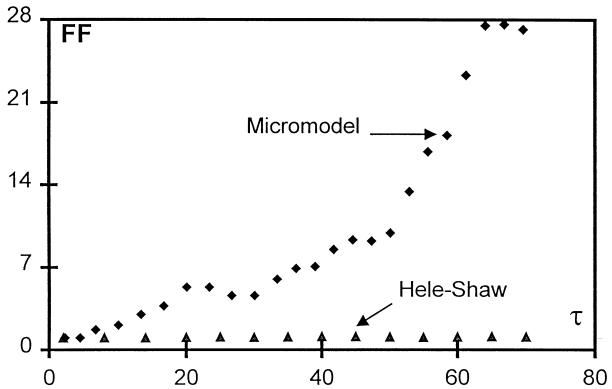

Fig. 6. Evolution of shape factor FF in a micromodel and a Hele-Shaw cell under identical thermodynamic conditions. These results have been obtained with fluid C and for a rapid depressurizing.

outer boundary radius, λ the fractal dimension of the gas cluster (=1.82 in 2D) and $k = R_g T/KM_s$, where R_g is the ideal gas constant, T the temperature and M_s the solute molecular weight. As shown in Fig. 7, this law is in rather good agreement with our experimental results. This is in fact quite surprising since in our case, the concentration fields are far from quasistatic (see, Section 3) and the size of the considered cluster is a priori too small for Eq. (1) to hold (see, Satik et al., 1995). It is also worth mentioning that the relationship $\Sigma \propto Ja^2 \tau FF$, with $FF = \Gamma^2/4\pi\Sigma$, is derived under the condition that the geometrical perimeter Γ can be assimilated to the effective perimeter for the mass transfer. In the case of fractal interfaces, it is well known that the effective (accessible) external perimeter is in fact smaller than the geometrical perimeter due to the screening of less advanced points of the interface by the most advanced ones, cf. Stauffer and Aharony (1992), Sapoval (1994). The evolution of FF for the micromodel experiment reported in Fig. 6 is qualitatively consistent with a developing fractal interface. Although the concept of shape factor as defined above permits us to illustrate the striking difference between the growth of a bubble in a porous medium and in a Hele-Shaw cell, it is clearly of limited interest in the case of a fractal cluster owing to the screening effect. It may be observed that the screening is presumably less effective for transient diffusion regimes, as is the case in our experiments, than for quasistatic concentration fields. However, this specific aspect has not been investigated in the present study.

Concerning the influence of the different parameters Ja, M, θ, and Bo on the growth of the gas cluster, the systematic experimental investigation carried out has led to the following main results:

1. In agreement with the scale analysis, the volume of the gas formed is proportional to Ja^2. As shown in Fig. 8, NSB $\propto ja^2\tau^\alpha$ (NSB = number of invaded bonds).
2. The value of α depends on the pressure lowering law, as in the case of homogeneous fluids. For a rapid depressurisation we have $2.3 > \alpha > 1.3$, with an average close to 1.5 as shown in Fig. 9, and for a linear decay $4.7 > \alpha > 3.5$, with an average close to $\alpha = 4$, cf. Dominguez (1997). Ranges of variation of α corresponding to these two experimental conditions ($M \to \infty$ and M = const.) arise from the different sizes of the gas clusters studied. As the

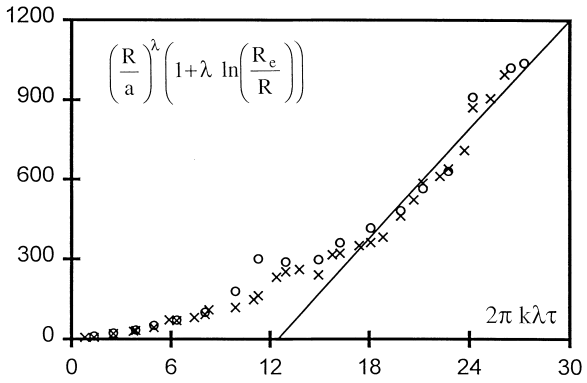

Fig. 7. Comparison of experimental gas-cluster growth (×, ○) with theoretical scaling law, Eq. (1) (straight line).

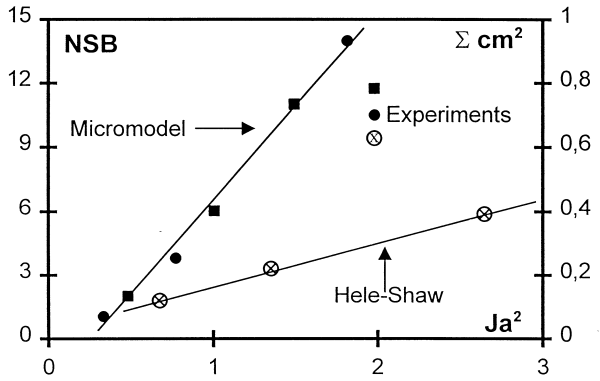

Fig. 8. Effects of micro-structure on bubble growth. Comparison of bubble growth in a Hele-Shaw cell with bubble growth in a micromodel as a function of Ja^2 (NSB is the number of invaded pores).

size of the cluster decreases, α tends to 1 through a transition zone relatively large compared to the scale of the micromodel. Thus, in spite of difficulties encountered in the analysis of the asymptotic growth rate of a single gas cluster under constant far field conditions (only gas clusters of small sizes were studied in order to avoid the influence of interactions between clusters), these results clearly show the strong influence of the microstructure on the growth of the gas phase in porous media. We have to remember that $\alpha = 1$ for a rapid depressurisation and $\alpha = 3$ for a linear decay of the pressure in homogeneous systems. They also lead to the same qualitative conclusions as for the bubble growth in homogeneous fluids, i.e. that α is greater for a linear decay of the pressure than for a rapid depressurisation (Wang and Bankoff, 1991).

3. Experimental investigation of the influence of wettability θ shows that this parameter does not influence significantly the growth rate of the gas clusters. For a rapid depressurisation

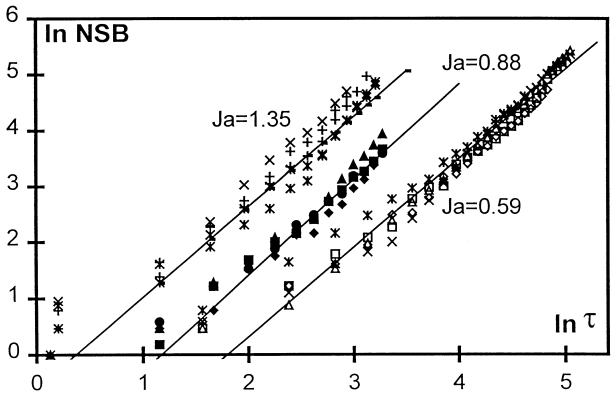

Fig. 9. Influence of Jacob number, *Ja*, on the growth law. The results of three experiments are reported for each Jacob number. $NSB \propto \tau^{1.62}$ for $Ja = 1.35$, $NSB \propto \tau^{1.61}$ for $Ja = 0.88$ and $NSB \propto \tau^{1.55}$ for $Ja = 0.59$ (NSB is the number of invaded pores). Each series of point with the same symbol corresponds to an experiment.

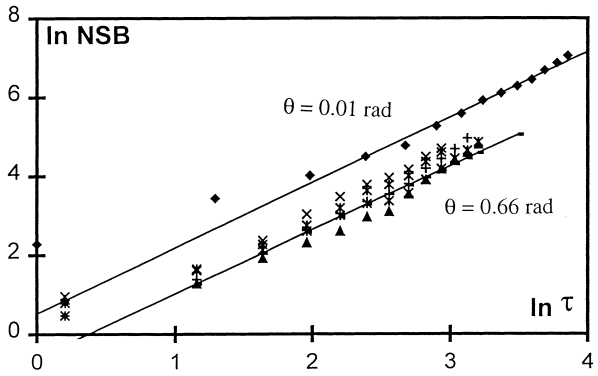

Fig. 10. Influence of wettability on the growth law for $Ja = 1.12$: $\mathrm{NSB} \propto \tau^{1.63}$ for $\theta = 0.66$ rad and $\mathrm{NSB} \propto \tau^{1.66}$ for $\theta = 0.01$ rad (NSB is the number of invaded pores). Each series of point with the same symbol corresponds to an experiment.

we have thus $\alpha = 1.63$ for $\theta = 0.66$ rad and $\alpha = 1.66$ for $\theta = 0.01$ rad, as shown in Fig. 10. The increase in wettability is associated with the increase of the interfacial area at pore scale between the gas and the liquid through the development of the liquid film along the pore walls. As discussed before, however, (Section 2), the effective area for the mass transfer is different from the geometrical interfacial area. In the diffusion regime considered here, the rate is controlled mostly by the large scale structures of the interface (tips) and not by the small ones. This may explain why the exponent of the growth law is practically not affected by the wettability. We note, however, that the wetting fluid remaining in the corner of the cross section of pores and in small cavities in the walls (as sketched in Fig. A1 in Appendix A) plays the role of a source term and tends to increase systematically the values of NSB (NSB = Number of invaded bonds).

4. Concerning the influence of the Bond number, i.e. of the gravity, we observed that this parameter has a strong influence on the growth rate, α taking the values 1.65, 1.98 and 2.33

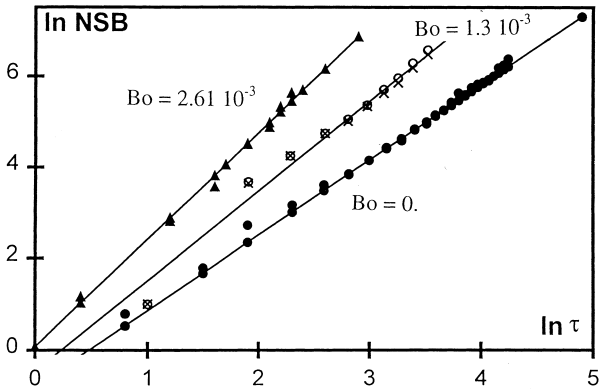

Fig. 11. Effect of gravity on the growth law for liquid C and $Ja = 1.09$. $\mathrm{NSB} \propto \tau^{2.33}$ for $Bo = 2.61 \times 10^{-3}$, $\mathrm{NSB} \propto \tau^{1.978}$ for $Bo = 1.31 \times 10^{-3}$ and $NSB \propto \tau^{1.65}$ for $Bo = 0$. (NSB is the number of invaded pores). Each series of point with the same symbol corresponds to an experiment.

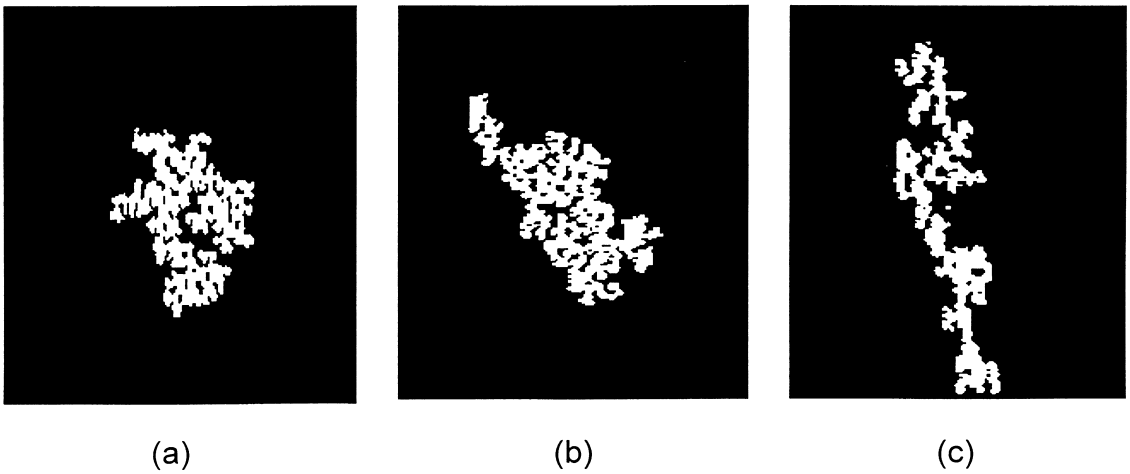

Fig. 12. Effect of gravity on the phase distribution for the same number of invaded pores (NSB $\cong$ 320). (a) $Bo = 0$; (b) $Bo \times 10^3 = 1.31$ and (c) $Bo \times 10^3 = 2.61$. Gravity vector is parallel to the right and left sides of micromodel (gas phase in white, liquid phase in black).

when the Bond number is respectively equal to: 0, 1.31×10^{-3} and 2.61×10^{-3}, as reported in Fig. 11. This is directly due to the fact that the gas cluster shape becomes more and more anisotropic as the Bond number increases (this is shown in Fig. 12). The cluster shapes depicted in Fig. 12 are consistent with invasion percolation patterns in the presence of a destabilizing gravity field, cf. Meakin et al. (1992) and Laurindo and Prat (1996).

3. Simulations

3.1. Pore network model

As mentioned before, earlier attempts to model bubble growth during pressure depletion in porous media were based on the identification of the porous medium with a continuum. When the porous medium is treated as an equivalent bulk system, the growth of an isolated 2D single bubble obeys the classical similarity scaling $R^2 \propto \tau$. In addition to the fact that this law does not agree with the results obtained in real porous media, previous visualisations showed the basic differences between growth in the bulk and in porous media and elucidated the reasons for this disagreement. These differences are exemplified by the disorder and the non-symmetry of gas clusters, resulting from the influence of the geometry and topology of the microstructure on the growth of the gas phase. Hence, as shown for others classes of two-phase flows in porous media by Lenormand et al. (1988), bubble growth in porous media cannot be adequately described by using a macroscopic continuum model. In such a situation, a discrete approach, i.e. a pore network model which is based on the modelling of mechanisms at pore scale, is more appropriate.

In fact, pore network models have been used for studying a great variety of transport phenomena in porous media, including liquid–vapor phase change phenomena, see for instance Prat (1993) and Laurindo and Prat (1996). Regarding the growth process studied in the present paper, a pore network model was developed by Li and Yortsos (1995). The main differences between the network model of Li and Yortsos and the simulator presented in the present paper lie in the diffusive transport modelling (see below) and the fact that our model accounts additionally for the presence of liquid films along the walls of invaded bonds. We would like to underline also that the effect of gravity is taken into account in our simulator and that our version allows the simulation of correlated microstructures. The porous medium is represented by a network of pores joined by bonds (throats), as sketched in Fig. 13(a). The pore and bond sizes are distributed randomly according to given distribution laws. The model is directly based on the observations of the cluster growth as explained below.

Observations from the transparent micromodel show that, after the initial gas bubble nucleates on the pore surface, it quickly detaches and migrates to the centre of the pore. Then the bubble grows until it fills the entire pore body. At this stage, additional mass diffusion increases the gas pressure and the interface invades another pore. From these observations two main stages can be distinguished in the cluster growth: (i) a slow pressurisation stage, during which the pressure in the cluster increases and the gas liquid

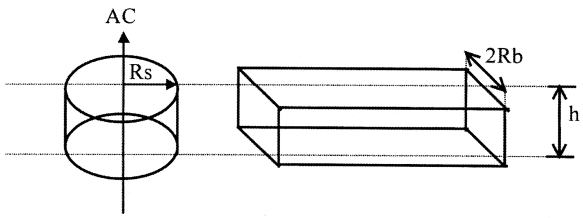

(a)

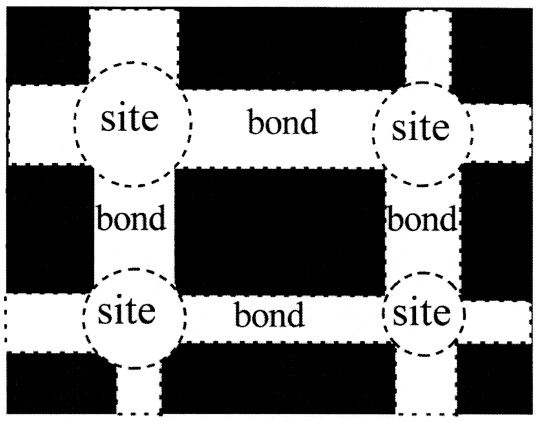

(b)

Fig. 13. Structure, sites and bonds of numerical network.

menisci move slightly to adjust their curvature to accommodate the pore geometry, (ii) a fast penetration stage immediately after a capillary barrier at a perimeter throat is exceeded. Following this stage, that corresponds to an evolution at almost constant mass, the volume of the cluster increases and the gas pressure quickly reduces to the adjacent liquid pressure as the invaded pore is occupied. After completely occupying a pore, the meniscus can invade a neighbouring bond if the corresponding capillary barrier is exceeded. Moreover, for perfectly wetting liquids, it is also observed that a film of liquid remains in the corners of the pores and bonds invaded by the gas. Consistently with these observations we developed a pore network automaton where both occupancy of pore and concentration fields are computed.

In the pore network automaton the porous medium is modelled by a two dimensional square lattice of pores and bonds. The pores provide the volumetric storage and the bonds control the capillary characteristics. Log-normal distributions are used to randomly assign bond and pore size on the numerical network. As in the micromodel, the lateral boundaries of the network are inaccessible to flow with the exception of two producing sites at opposite ends.

As in the experiments, the network is initially occupied by a supersaturated liquid and the system has a uniformly distributed initial pressure Po and initial concentration of CO_2. The simulation starts by reducing the liquid pressure either by a sharp step ΔP or at a specified rate $m = -\mathrm{d}P/\mathrm{d}t$. In the simulations, we assume that we are after the nucleation of one bubble and that the pore that contains the nucleation site is fully occupied by the gas at pressure P_g equal to the pressure of the liquid $P_\infty = Po - \Delta P$ (neglecting the capillarity of the pore body). At the same time, the bubble is surrounded by four liquid saturated bonds and the concentration C_s of the dissolved gas at the gas–liquid interface is given by $C_s = KP_\infty$, where P_∞ is the system pressure. As in Li and Yortsos (1995), the hypotheses that sustain these approximations are that thermodynamical equilibrium applies at the gas–liquid interface at all times (note that the Kelvin effect is neglected) and that the relation between the liquid pressure and the concentration is linear.

The transient diffusive mass transfer of CO_2 in the liquid that drives the gas cluster growth, and the invasion of the network is computed by using explicit analytical mass transfer laws adapted from classic solutions of transient diffusion processes, cf. Crank (1957). One such law is sufficient for the less wetting liquids, since in this case the gas–liquid interface is restricted to the cross section of bonds. Two laws are considered in the case of the more wetting liquids because of the presence of liquid films along the bond walls. These laws, given in Appendix A, allow one to compute the mass flux between the liquid and the gas in each interfacial bonds. A more traditional way for computing a concentration field governed by a diffusion equation in the network approach is to use a finite difference or finite volume discretisation, see for instance Li and Yortsos (1995) or Prat (1993). This requires the repeated solution of a linear system of equations, which is CPU time consuming. The method proposed in this paper avoids this problem. However, this is clearly an approximation whose validity deserves to be explored in some details (for instance through comparisons with the discretisation approach). In this paper, we simply proceeded by comparison with the experimental results (see below).

By expressing the mass flux balance at each gaseous node as a function of time, one obtains the evolution of the mass of the gas phase, and of the pressure in the gas cluster as a function

of time:

$$\Delta n_{\mathrm{T}} = \Sigma_{\mathrm{B}} \Delta n(i,j)_{\mathrm{B}} + \Sigma_{\mathrm{F}} \Delta n(i,j)_{\mathrm{F}} \tag{2}$$

$$\Delta P_{\mathrm{G}} = \Delta n_{\mathrm{T}} RT / V_{\mathrm{G}} P_{\mathrm{G}}(t+\Delta t); \quad P_{\mathrm{G}}(t+\Delta t) = \Delta P_{\mathrm{G}} + P_{\mathrm{G}}(t) \tag{3}$$

where $\Sigma_{\mathrm{B}} \Delta n(i,j)_{\mathrm{B}}$, and $\Sigma_{\mathrm{F}} \Delta n(i,j)_{\mathrm{F}}$, are the CO_2 mass flux from the bonds B and the liquid films F belonging to the interface between the gas cluster and the surrounding liquid phase. $V_{\mathrm{G}} = V_{\mathrm{G}}(t)$ is the volume of the gas cluster at time t. If the pressurisation $P_{\mathrm{G}}(t+\Delta t)$ is greater than $P_{\infty}(j) + P_{\mathrm{C}}(i,j)$, where $P_C(i,j)$ is the capillary pressure of an arbitrary bond (i,j), the interface advances and occupies the site j (note that bonds belonging to isolated trapped liquid clusters cannot be invaded as in standard invasion percolation with trapping). The volume of the gas cluster at time $t+\Delta t$ is next calculated using the mass balance derived from the state equation: $\Delta n = 1/RT\{(V_{\mathrm{G}} P_{\mathrm{G}})(t+\Delta t) - (V_{\mathrm{G}} P_{\mathrm{G}})(t)\}$. Based on the difference $\Delta t = \Delta n - \Delta n_T$, additional iterations are taken on the assumed gas volume until a convergence tolerance defined by $\Delta t < 10^{-13}$ is reached. In this mode of interface advance, the time required for the bond invasion is determined from the previous mass diffusion equations and the gas cluster grows according to the invasion percolation rules, i.e., the perimeter bonds are invaded one at a time in such a way that the largest perimeter bond (in the absence of gravity) is always invaded first.

At the end of each time step, a check is made to determine whether the conditions required for additional perimeter throats to be penetrated are satisfied. When all the pores in the gas cluster are fully occupied and new equilibrium conditions exist, the new average CO_2 concentration in the liquid saturated bonds surrounding the gas cluster is determined by the following expression: $(\Delta Cs(i,j))(t+\Delta t) = (\Delta Cs(i,j)(t) V_{\mathrm{L}}(i,j) - \Delta n(i,j)_T)/V_{\mathrm{L}}(i,j)$, where V_{L} is the volume of the liquid in the i,j, bonds. V_{L} is given by $V_{\mathrm{L}}(i,j) = V_{LD}(i,j) + V_{\mathrm{FP}}(i,j)$, where V_{LD} and V_{FP} are the volume displaced in the considered bond and the volume of liquid film remaining along the walls of the bond, respectively. $\Delta Cs(i,j)(t+\Delta t)$ corresponds to the new initial supersaturation condition used for calculating the new mass transfer step from the liquid to the gas. As detailed in Dominguez (1997), this expression is only valid for V_{LD} = volume of new neighbours bonds (NNB) created during the considered growth stage. When V_{LD} is less than volume of new neighbours NN, the average supersaturation in the surrounding liquid saturated bonds is computed from the following mass balance: $\Delta Cs(i,j)(t+\Delta t) = (V_{\mathrm{LD}} \Delta Cs(i,j)(t+\Delta t) + (\mathrm{NVV} - V_{\mathrm{LD}}) K \Delta P)/\mathrm{NN}$, which takes into account the increase of the interfacial area between the gas cluster and the surrounding liquid at time $t+\Delta t$.

As first proposed by Wilkinson (1984) and subsequently used by several authors (see Laurindo and Prat, 1996 among others), gravity effects can be easily taken into account by defining an appropriate bond invasion potential, which depends not only on the width of the throat (as in the no-gravity case) but also on the relative position of the throat in the gravity field. Additional details concerning the topological rules governing the pore occupancy as well as the computational algorithm can be found in the thesis of Dominguez (1997).

3.2. Experiments versus numerical simulations

In this section, we present the results obtained by means of two dimensional numerical

simulations and the comparisons of these results with the experiments. The network used in the simulations is constructed by using a classical Monte-Carlo simulation in which the size of an element (site or bond) is selected at random from the cumulative pore radius and duct width distributions of the micromodel (Cruz et al., 1989). This network has the same characteristics as the micromodel, i.e., the same porosity $\varepsilon = 0.58$, the same length of bond (corresponding to the length of ducts $a = 0.1$ cm), the same thickness $h = 700$ μm, and the same pores and ducts sizes distributions. The geometry of pores and ducts is approximated by cylindrical sites and rectangular bonds, as shown in Fig. 13(a). The fluid physical properties are those of the fluids used in the experiments.

Experimental and simulated results of pore volume–time curves NSB (τ), which represents the overall system behaviour, as well as of growth patterns, which provide local details, are compared in Figs. 14–16. Regarding the evolution of the volume of the gas phase as a function of time, a rather good agreement is found between the experiments and the simulations both in Fig. 14 corresponding to an abrupt pressure decrease and in Fig. 15 corresponding to a constant pressure decline rate.

Fig. 16 shows the comparison between the experimental and numerical patterns for one of the experiments. The two patterns share many topological characteristics (irregular and ramified shapes, including disconnected liquid clusters) but are not identical. These differences in the microscale result from the differences between the spatial localisation of pores and ducts on the experimental and numerical networks (only the pore and bond size distributions are identical on both networks). As emphasised in Li and Yortsos (1995), these differences in localisation produce different occupancy sequences and therefore, preclude the automaton from

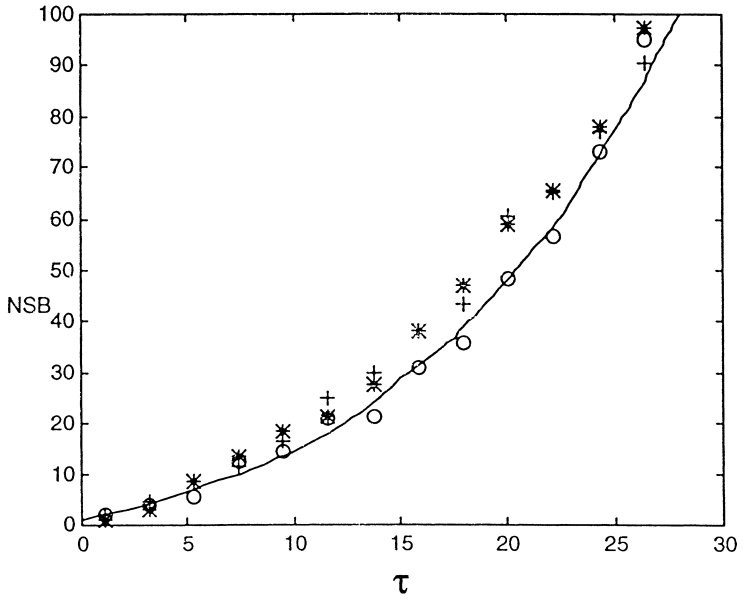

Fig. 14. Number of invaded bonds (NSB) as a function of time in a single cluster. Comparison between numerical results (solid line) and experimental data (∗, ×, ○) ($Ja = 0.89$). $Ca = 4.81 \times 10^{-7}$, $\theta = 0.66$, fluid C. Rapid depressurizing.

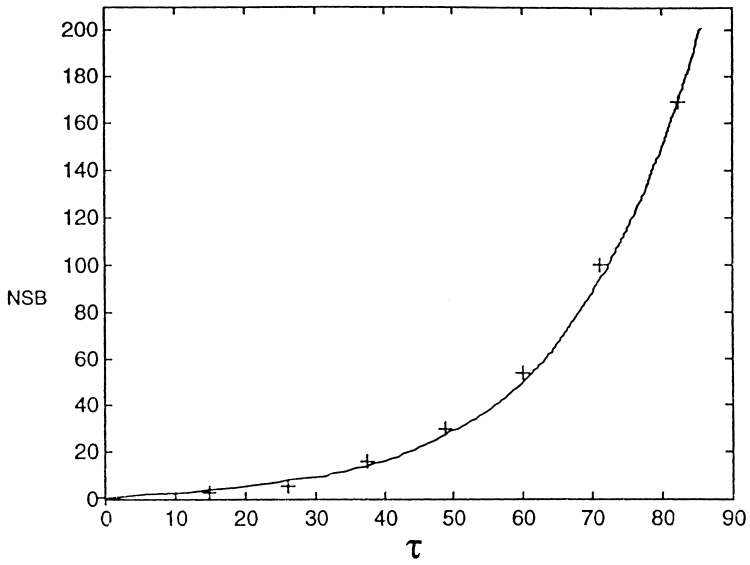

Fig. 15. Number of invaded bonds (NSB) as a function of time in a single cluster. Comparison between numerical results (full line) and experimental data (+), ($\Delta P_b/P_{sat} = 0.41$ and $M \cong 5 \times 10^{-3}$). Fluid *B*. $Ca = 5.81 \times 10^{-7}$.

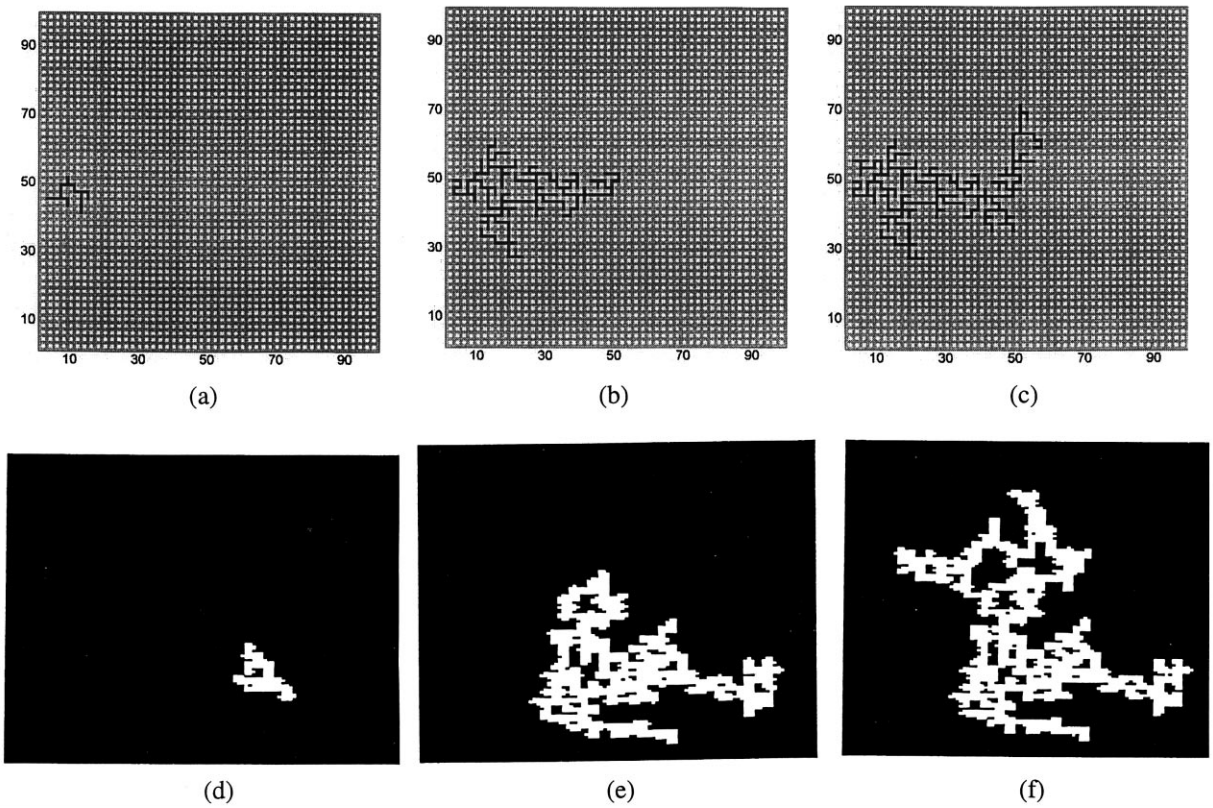

Fig. 16. Typical evolution of a gas cluster. Top: numerical results for: (a) NSB = 16; (b) NSB = 146; (c) NSB = 201. Bottom: experimental results for: (d) NSB = 16; (e) NSB = 146; (f) NSB = 204. $\Delta P_b/P_{sat} = 0.41$, $M \cong 5 \times 10^{-3}$, fluid *B*. $Ca = 5.81 \times 10^{-7}$.

accurately matching the microscopic details of bubble growth. Therefore, we conclude that the dominant mechanisms are correctly simulated in the range of parameters studied and that the automaton is able to match the most important aspects of phase growth. Consequently, it will be used to explore the sensitivity of the phenomenon to different parameters in the following.

3.3. Sensitivity study

This section concerns the investigation of the influence of the following parameters: Jakob number, surface tension, wettability, Bond number, pressure decline rate and finally the microstructure on the growth of a single gas cluster.

The results concerning the influence of Jakob number on the gas saturation ($S \propto \mathrm{NSB/NT}$, where NT is the total number of sites and bonds in the micromodel) are presented in Fig. 17. As can be seen, many aspects of these results are not only qualitatively but also quantitatively in agreement with the experiments. In accordance with the experiments, the growth law takes the form

$$\mathrm{NSB} \propto Ja^2 \tau^{\alpha} \tag{4}$$

with α independent of Ja. The simulations also show the existence of a transition zone corresponding to the evolution of α from 1 to 2.13, which corresponds to the investigated range of variation of the gas cluster size NSB. This last result is in agreement with the values obtained experimentally with the micromodel. It is worth noting that the transition zone time scales deduced from the simulations ($0 < \ln \tau < 3.5$) are also in agreement with the experiments.

As the capillarity directly control all entrances of the interface bonds, the greater the surface

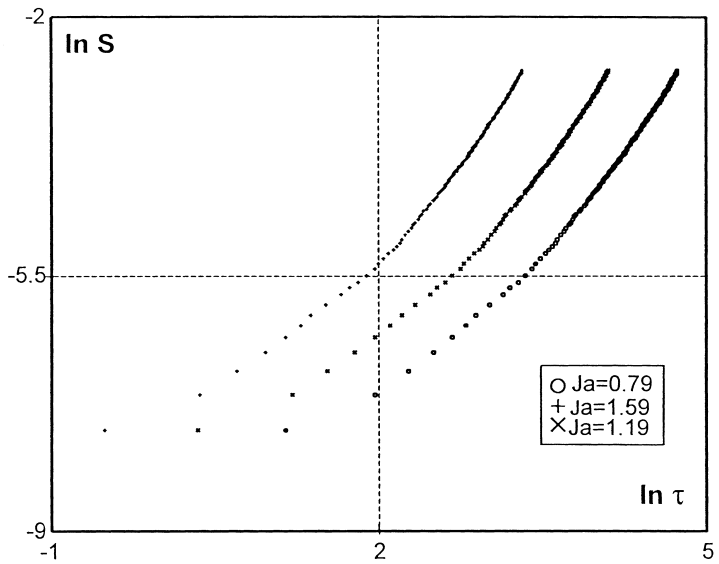

Fig. 17. Pore network simulation. Influence of the Jacob number on the growth law of fitted from numerical results ($\theta = 0.63$) $S \propto \tau^{2.13}$.

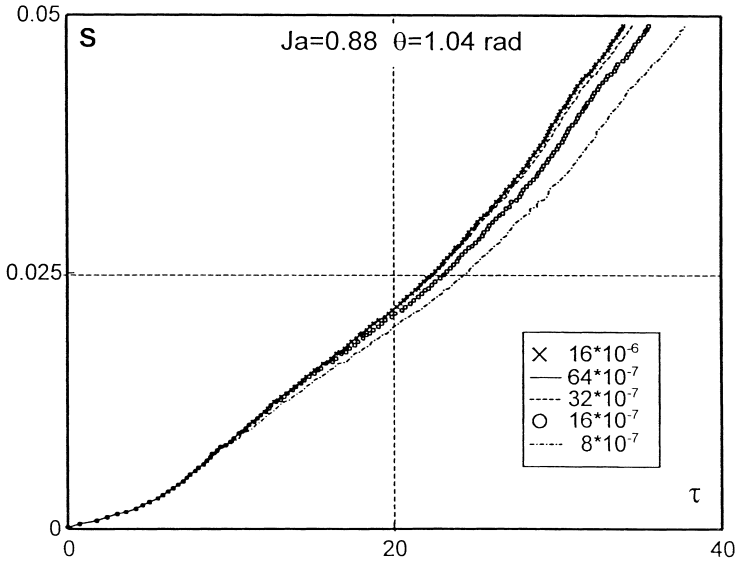

Fig. 18. Pore network simulation. Influence of Capillary number.

tension, the higher is the pressure difference required to penetrate the bonds. As this difference is itself controlled by mass transfer, i.e. by the number of the CO_2 molecules contained in the gas phase, the effect of this parameter is then to modify the growth rate of the gas cluster, i.e., the values of the exponent α in Eq. (4) as illustrated in Fig. 18.

The influence of the wettability, which leads to the spreading of the liquid along the corners and surface of pores occupied by the gas phase, is illustrated in Fig. 19. As can be seen, this

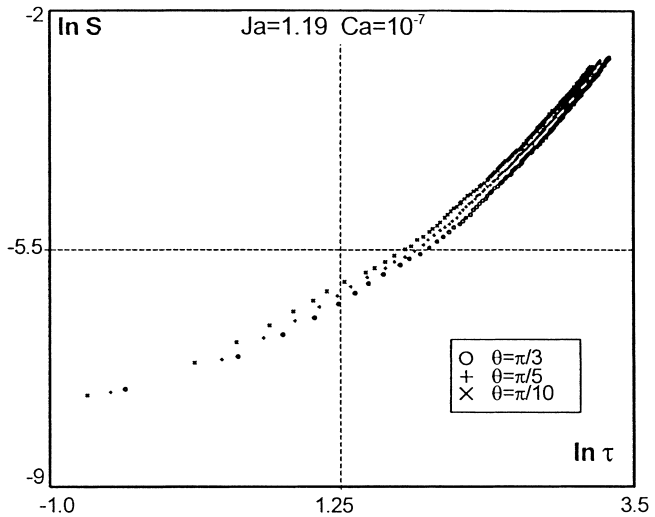

Fig. 19. Pore network simulation. Influence of the wetting properties at constant *Ca* and *Ja*. Best fits give $S \propto \tau^{2.18}$ rad, for $\theta = \pi/3$ rad, $S \propto \tau^{2.11}$ for $\theta = \pi/5$ and $S \propto \tau^2$ for $\theta = \pi/10$ rad.

parameter does not modify the growth of the gas phase as a function of time; α remains constant and approximately equal to 2.1 irrespective of the values of θ. In fact the effect of the wettability is exclusively restricted to the monotonic increase of NSB. This result is in agreement with the experiments. As a local (pore level) examination of mass transfer shows, this effect can be considered as a source effect owing to the liquid remaining in the extreme corners of the cross section of pores and micro-cavities of the walls.

Fig. 20 shows the influence of the Bond number on the growth phenomenon. As in the experiments, this parameter has a significant influence on the evolution of volume of gas formed after the pressure lowering, the exponent varying from 2.0 to 2.2 while the Bond number varies from 0 to 5.1×10^{-3}. The simulated patterns of gas clusters shown in Fig. 21 and the local analysis of mass transfer along the gas liquid interface help to understand this influence. The main factors are: (i) The elongation of the cluster in the direction of the gravity when the Bond number increases, i.e., the increase of the effective accessible perimeter with the anisotropy of the cluster. (ii) The movement of the interface towards the region where the supersaturation is less affected by the mass transfer. As confirmed numerically in Dominguez (1997), the latter effect indeed leads to greater local mass transfers through the liquid bonds adjacent to the region of the cluster that is the most advanced towards the upper edge of the network.

The results concerning the influence of the pressure decline rate M on the evolution of the volume of gas are presented in Fig. 22. Again in agreement with the experiments, we note that the larger is the pressure decline rate, the faster is the bubble growth, which remains consistent with the results in the bulk.

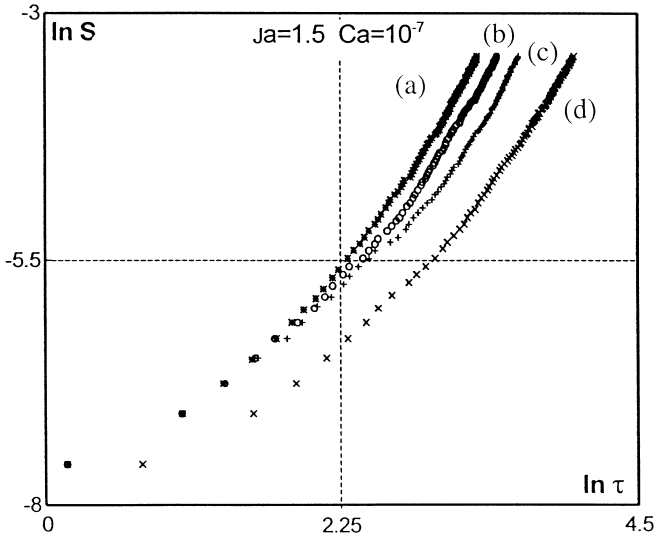

Fig. 20. Pore network simulation. Effect of gravity on the cluster growth law. Results are shown for: (a) $Bo \times 10^3 = 5.15$; (b) $Bo \times 10^3 = 2.61$; (c) $Bo \times 10^3 = 1.31$; and (d) $Bo = 0$. Best fits give: $S \propto \tau^{2.23}$ for (a), $S \propto \tau^{2.22}$ for (b), $S \propto \tau^{2.17}$ for (c) and $S \propto \tau^{2.06}$ for (d).

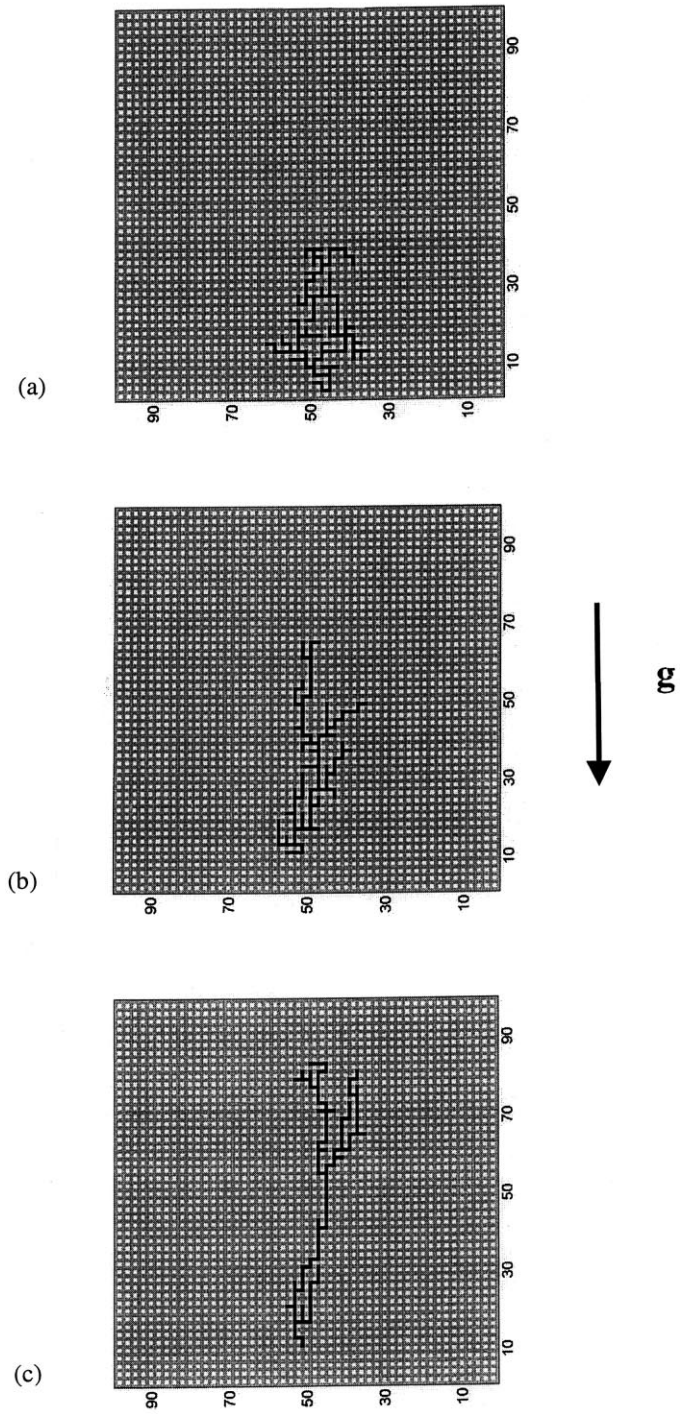

Fig. 21. Pore network simulation. Influence of Bond number on phase distribution. Results are shown for NSB (Number of Invaded Bonds) = 100: (a) $Bo = 0$, (b) $Bo \times 10^3 = 2.61$, (c) $Bo \times 10^3 = 5.15$ (gas phase in black, liquid phase in grey).

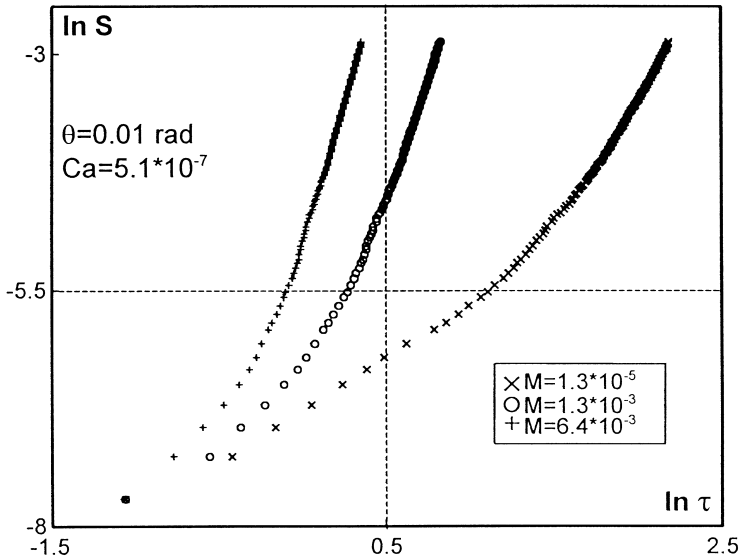

Fig. 22. Pore network simulation. Influence of pressure decline rate M on the growth law. Best fits give: $S \propto \tau^{5.97}$, $S \propto \tau^{4.99}$ and $S \propto \tau^{2.71}$.

Preliminary results regarding the influence of bond/pore size correlations on the growth rate of gas clusters of small size: (NSB = 1–200) were also obtained as a function of time. To this end, we used the procedure defined in Cruz et al. (1989). This procedure, which is based on the principle that the size of a bond is necessary smaller than the size of the two pores adjacent to the bond, permits to introduce bond/pore size correlations. The degree of correlation increases with the overlap between the bond size and the pore size distributions (a fully random network corresponds to zero overlap). The cases we considered correspond to the bond and pore size distribution depicted in Fig. 23. Significant differences concerning the growth rates are observed when the overlapping of pore and bond size distributions increases, as can be seen from Fig. 24. The growth rate seems very sensitive to the evolution of the microstructure and increases significantly with the overlapping. This result is certainly due to the structural heterogeneities which develop in the network when the degree of correlation between the sizes of neighbouring elements increases. This deserves to be explored further, both experimentally and numerically, through a thorough statistical study.

4. Conclusion

The present work continues and extends the work of El-Yousfy et al. (1991) and El-Yousfy (1992), concerning the nucleation and the growth of a stationary gas bubble due to solute diffusion in porous media. While in the preceding investigations attention was focussed only on the experimental study of the influence of the supersaturation and pressure decline rate on the

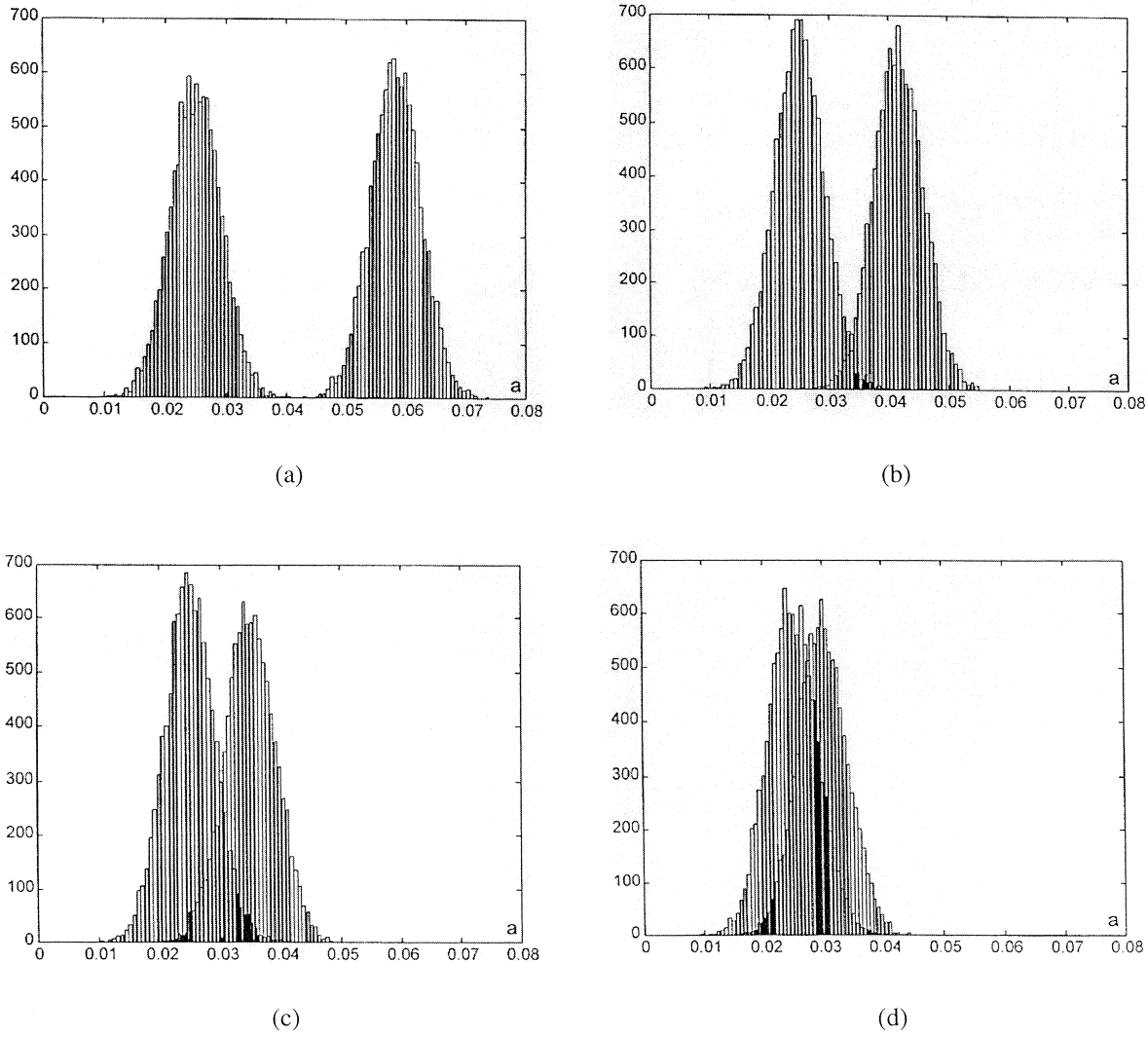

Fig. 23. Size distributions of the constitutive elements of the correlated numerical networks. The overlap between distributions increases from (a) to (d).

formation and the growth of the gas phase, in the present work, we additionally analysed experimentally and numerically the effects of wettability, gravity and microstructure on these phenomena.

While the observations confirmed the decisive role of a capillary trapping mechanism on the formation of bubbles, i.e. the pre-existence of microbubbles trapped in cavities or roughness on the solid surface, analysis of the growth rate of an isolated single gas bubble showed that this phenomenon is different in porous media than in the bulk. As a matter of fact, contrary to compact growth in the bulk, the growth pattern of the gas phase in porous media is disordered

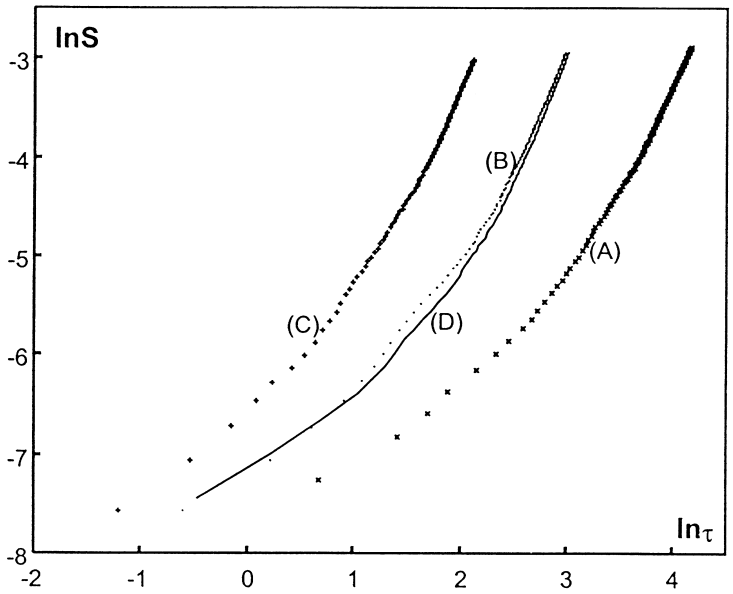

Fig. 24. Pore network simulation on correlated network. Growth law for the various networks corresponding to the pore and bond size distribution shown in Fig. 23. Best fits give (from a to d): $S \propto \tau^{2.40}$, $S \propto \tau^{2.57}$, $S \propto \tau^{2.54}$ and $S \propto \tau^{2.50}$.

and the growth rate of an isolated gas cluster is different from the growth rate of an isolated single bubble. This difference comes from the particular evolution of the gas liquid interface which is strongly influenced by the microstructure, i.e., by the local values of the capillary pressure in each pore. In agreement with Li and Yortsos (1995), isolated clusters are found to grow in a manner similar to the invasion percolation process. As a result, the volume of a single gas cluster tends to grow faster in porous media than in the bulk: $\mathrm{NSB} \propto Ja^2\tau^{\alpha}$, with the exponent α greater than the values corresponding to the usual compact growth, depending on the pressure lowering law and Bond number.

A 2D numerical simulator was then used for a sensitivity study. Based on a set of hypotheses derived from the experimental visualisations, this pore network simulator was first tested by comparing experimental and numerical results. The comparisons showed good agreement as far as the overall system behaviour is concerned. The sensitivity study confirmed the growth law $\mathrm{NSB} \propto Ja^2\tau^{\alpha}$, and the influence of different parameters (pressure decline laws: Ja, M; wettability: θ; gravity: Bo) on the values of α. In addition, this tool was used to investigate the effects of the surface tension and of some characteristics of the microstructure on the growth law. As expected, α decreases as the surface tension increases. Concerning the influence of the correlation between the bond and pore sizes, preliminary results presented here show a significant influence on the growth rates. These results have to be confirmed experimentally and/or through a statistical numerical study. From a numerical point of view, some refinement of the automaton are under consideration. In particular, it would be

interesting to develop a 3D version of the simulator, especially for the situations where the gravity effects are important.

Acknowledgements

A. Dominguez was supported by a grant from CONACyT and UAMI (Mexico). The authors wish to express their gratitude to the late Prof. V. Mayagotia for stimulating the work reported in this paper. They are indebted to two anonymous referees for their critical review and constructive suggestions on the original manuscript. The authors are grateful to John Georgiadis for a careful reading of the manuscript.

Appendix A. Computation of diffusive transport in the liquid

The transport of CO_2 in the liquid phase is computed by assuming a one-dimensional transient diffusive transport through each bond occupied by the liquid phase surrounding the gas cluster, and through the liquid films on the walls of bonds occupied by the gas phase.

A1. Abrupt pressure lowering

For an abrupt lowering of the pressure, the mass flux $\Delta n(i,j)$ between the surrounding bonds (i,j) and the gas cluster from the moment t to the moment $t+\Delta t$ is computed by (see Crank, 1957):

$$\Delta n(i,j)_B = 2As(i,j)\Delta C(i,j)\left\{(D/\pi)^{0.5}\left((t+\Delta t)^{0.5}-(t)^{0.5}\right)\right\} \tag{A1}$$

where $As(i,j)$ is the area of the cross section of the bond (i,j) and $\Delta C(i,j)$ the CO_2 supersaturation within this bond. In order to obtain Eq. (A1), the liquid bond is treated as a semi-infinite medium. When a liquid film is present along the bond walls, the mass flux between the film and the gas contained in the bond is computed by (see Crank, 1957):

$$\Delta n(i,j) = Vfp(i,j)\Delta C(i,j)/2\left\{\sum_q (8/\left((2q+1)^2\pi^2\right)\exp\left(-D(2q+1)^2\pi^2/4hp^2\right) \times (\exp(t+\Delta t)-\exp(t)\right\} \tag{A2}$$

where $Vfp(i,j)\Delta C(i,j)/2$ represents the mass of CO_2 contained in the (i,j) bond and q is an integer. To derive Eq. (A2), the liquid film, the thickness of which is calculated from the results of Lenormand (1981), is identified to a liquid layer of uniform thickness hp bounded on one side by an impervious plane with a mass flux equal to zero (see Fig. A1).

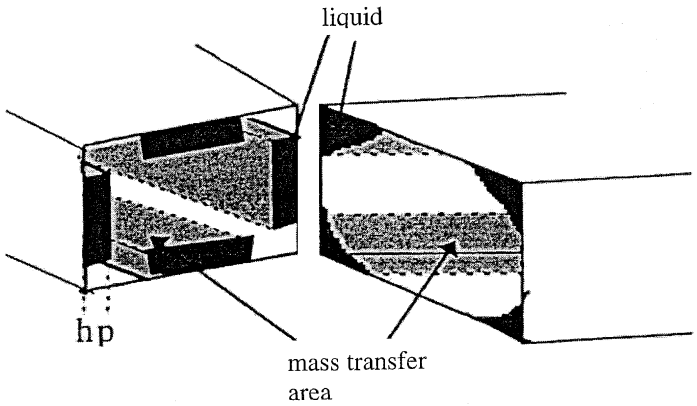

Fig. A1. Liquid corner flow in a duct invaded by the gas phase.

A2. Linear pressure decay

In the case of a linear decay of the pressure the system pressure is described by a series of equal pressure steps ΔP. During each step, the process is simulated following the same rules as for an abrupt lowering of the pressure, but the mass transfer laws (A1) and (A2) between the liquid and the gas are modified to take into account the non-stationary boundaries conditions along the gas-liquid interface. For a 1D problem, these laws are well known (Crank, 1957). They read, respectively, for the bonds and the films:

$$\Delta n(i,j)_{\mathrm{B}} = 2As(i,j)(D/\pi)^{1/2}\left\{Cs(i,j)\left(\sqrt{t}+\Delta t-\sqrt{t}\right)+2/3\ Ke\ m\left((t+\Delta t)^{3/2}-(t)^{3/2}\right)\right\} \tag{A3}$$

and

$$\begin{aligned}\Delta n(i,j)_{\mathrm{B}} = {} & Vsp(i,j)Csp(i,j)/2\left\{\sum_{q=0}^{\infty}8/(2q+1)^2\pi^2\ \exp\left(-\left(D(2q+1)^2\pi^2/4(hp)^2\right)\right.\right.\\ & \left.\left.\times\left(\exp(t+\Delta t)-\exp(t)\right)\right\}+Ke\ m(hp)(t+\Delta t-t)+\left(Ke\ m(hp)^3/D\right)32/\pi^4\sum_{q=0}^{\infty}\\ & \times\left(\exp\left(-D(2q+1)^2\pi^2/4(hp)^2\right)\left(\exp(t+\Delta t)-\exp(t)\right)\right)/(2q+1)^2\end{aligned} \tag{A4}$$

As shown in Dominguez (1997), due to the constant time of the growth phenomena, use of these laws is, however, only valid for $M = ma^2/PoD < 1$, i.e. for slow pressure lowering.

References

Betata, S.A., 1998. Les écoulements polyphasiques aux abords des puits dans les gisements d'hydrocarbures. Ph.D. thesis, Universite Paris 6, France.

Crank, J., 1957. The Mathematics of Diffusion. Clarendon Press, Oxford.

Cruz, M.J., Mayagoitia, V., Rojas, F., 1989. Mechanistics studies of capillary processes in porous media. Part II: Construction of porous networks by Monte-Carlo methods. J. Chem. Soc. Faraday Trans. 1, 85, 8, 2079–2086.

Dominguez, A., 1997. Formation d'une phase gazeuse par decompression d'une solution binaire en milieu poreux. Ph.D. thesis, Institut National Polytechnique de Toulouse, France.

El-Yousfy, A., Zarcone, C., Bories, S.A., Lenormand, R., 1991. Mécanisme de formation d'une phase gazeuse par detente d'un liquide en milieu poreux. C.R.A.S. Paris Série 2, 1093–1099.

El-Yousfy, A., 1992. Contribution à l'étude des mecanismes de formation d' une phase gaseuse par détente d'une solution binaire liquide gas en milieu poreux. Ph.D. thesis, Institut National Polytechnique, Toulouse, France.

Hunt Jr, E.B., Berry Jr, V.J., 1956. Evolution of gas from liquids flowing through porous media. AIChEJ 2, 560–567.

Kashchief, D., Firoozabadi, A., 1993. Kinetics of the initial stage of isothermal gas phase formation. J. Chem. Phys 98, 1.

Laurindo, J.B., Prat, M., 1996. Numerical and experimental network study of evaporation in capillary porous media. Phase distributions. Chem. Eng. Sci 51, 5171–5185.

Lenormand, R., 1981. Deplacements polyphasiques en milieu poreux sous l' influence des forces capillaires. Etude experimentale et modelisation de type percolation. Ph.D. thesis, Institut National Polytechnique de Toulouse, France.

Lenormand, R., Touboul, E., Zarcone, C., 1988. Numerical models and experiments on immiscible displacements in porous media. J. Fluid Mech 189, 165–167.

Li, X., 1993. Bubble growth during pressure depletion in porous media. Ph.D. thesis, University of Southern California, Los Angeles, USA.

Li, X., Yortsos, Y.C., 1994. Theory of multiple bubble growth in porous media by solute diffusion. Chem. Eng. Sci 50, 1247–1271.

Li, X., Yortsos, Y.C., 1995. Visualization and simulation of bubble growth in pore networks. AIChE Journal 41, 214–222.

Meakin, P., Feder, J., Frette, V., Jossang, T., 1992. Invasion percolation in a destabilizing gradient. Phys. Rev A 46, 3357–3368.

Moulu, J.C., 1989. Solution-gas drive: experiments and simulation. J. Petr. Sci. Eng 2, 379–386.

Prat, M., 1993. Percolation model of drying under isothermal conditions in porous media. Int. J. Multiphase Flow 19, 691–704.

Sapoval, B., 1994. General formulation of Laplacian transfer across irregular surfaces. Phys. Rev. Lett 73, 3314–3316.

Satik, C., Li, X., Yorsos, Y.C., 1995. Scaling of single-bubble growth in a porous medium. Phys. Rev. E 51, 3286–3295.

Scriven, L.A., 1959. On the dynamics of phase growth. Chem. Eng. Sci 10, 1–12.

Stauffer, D., Aharony, A., 1992. Introduction to Percolation Theory. Taylor and Francis, London.

Szekely, J., Martins, G.P., 1971. Non equilibrium effects in the growth of spherical gas bubbles due to solute diffusion. Chem. Eng. Sci 26, 147–159.

Tong, W., Bar-Cohen, A., Simon, W., You, S., 1990. Contact angle effects on boiling incipience of higly-wetting liquids. Int. Jour. Heat and Mass Trans 33, 91–103.

Wang, C.H., Dhir, V.K., 1993. On the gas entrapment and nucleation site density during pool boiling of saturated water. Jour. Heat Trans 115, 670–679.

Wang, G., Bankoff, G., 1991. Bubble growth on a solid wall in a rapidly-depressurized liquid pool. Int. J. Multiphase Flow 17, 425–437.

Wilkinson, D., 1984. Percolation model of immiscible displacement in the presence of buoyancy forces. Phys. Rew. A 30, 520–531.

Yang, S.R., Kim, R.H., 1988. A mathematical model of pool boiling nucleation site density in terms of surface characteristics. Int. Jour. Heat and Mass Trans 31, 1127–1135.

Yortsos Y.C., Parlar M., 1989. Phase change in binary systems in porous media. Application to solution gas drive. SPE paper 19697 SPE meeting, San Antonio, TX.

Zettlemoyer, A.C., 1969. Nucleation. Marcel Decker, New York.